J Mater Sci (2008) 43:4091–4098
DOI 10.1007/s10853-007-2239-9

REES RAWLINGS FESTSCHRIFT

Two-dimensional (2D) and three-dimensional (3D) analyses of plasma-sprayed alumina microstructures for finite-element simulation of Young's modulus

**O. Amsellem · K. Madi · F. Borit · D. Jeulin ·
V. Guipont · M. Jeandin · E. Boller · F. Pauchet**

Received: 17 July 2007 / Accepted: 18 October 2007 / Published online: 3 April 2008

Abstract Thermally sprayed ceramic coatings such as plasma-sprayed alumina exhibit a composite microstructure actually due to the presence of defects such as pores, inter-lamellar and intra-lamellar cracks. These second phase-typed features influence the mechanical behaviour of the coating dramatically. In this study, a microstructure simulation of plasma-sprayed alumina was developed for the optimizing of component properties such as electrical tool used in the oil industry. This approach consisted of a finite-element analysis of mechanical properties from simulated microstructures. Several composite microstructures were tested from air plasma spraying of alumina. Various degrees of porosity and cracks could be obtained from different spraying conditions. Every composite microstructure was studied using a quantitative image analysis of scanning electron microscope (SEM) cross-sections. A finite-element model based on the actual microstructure was developed. First, two-dimensional (2D) finite elements meshes were created from SEM images of microstructures. Then, in order to have a realistic representation of the three-dimensional (3D) microstructure, pictures were obtained using X-ray microtomography. Volume tetrahedral grids were generated to simulate the properties of alumina coatings. This work studies the contribution of every part of the alumina coating to the final properties and shows potentials and limitations of the 2D and 3D computational approach.

Introduction

Thermal spraying is a prominent process for depositing low-cost high-performance dielectric coatings such as those made of pure alumina (Al_2O_3). Al_2O_3 is used extensively for its electrical insulating properties because of its high dielectric strength [1]. Thermal spraying is a deposition process in which molten particles impact at a high velocity, spread and solidify onto a substrate to form thin lamellae. Consequently, thermally sprayed alumina coatings show a composite microstructure due to the presence of defects such as pores, inter-lamellar and intra-lamellar cracks. These defect origins are multiple. First, build-up defects and entrapped gas generate-specific inter-lamellar cracks and pores. Second, intra-lamellar microscopic cracks may be achieved due to rapid solidification after spreading, especially for ceramic materials. The combination of these features generates an interconnected network of pores and cracks. These second phase-typed features influence the mechanical behaviour and the electrical insulation of the coating dramatically [2, 3].

In order to know their influence, some authors already described physical properties as a function of coatings microstructure for plasma processing [4–6]. This work was carried out to go into this microstructure-properties approach for coating development. However for plasma-sprayed

---

O. Amsellem (✉) · K. Madi · F. Borit · D. Jeulin ·
V. Guipont · M. Jeandin
Ecole des Mines de Paris—ParisTech, Centre des Materiaux
(CNRS 7633), Centre de Compétence en Procédés de Projection
(C2P), BP 87, 91003 Evry Cedex, France
e-mail: olivier.amsellem@ensmp.fr

E. Boller
ID19 Topography & Microtomography Group, European
Synchrotron Radiation Facility, 6, rue Jules Horowitz,
F-38043 Grenoble, France

F. Pauchet
Schlumberger, Riboud Product Center, 1, rue Henri Becquerel,
92140 Clamart, France

coatings, only a few attempts can be noticed because of the intricacy of the involved microstructure [7, 8]. This work was based on the study of composite microstructures (alumina and porosity) obtained by air plasma spraying (APS). Methods can be envisaged to investigate into the mechanical behaviour of the coating, i.e. first, a model based on a statistical study of composite phases [9] and, second, a model based on the actual coating microstructure [7, 8]. The first model does not involve any features of the microstructure. In contrast, this contribution shows a finite-element model (FEM) based on the actual microstructure, which allows the characterization of all the composite microstructure features and that of mechanical properties of coating.

In a preliminary stage, a two-dimensional (2D) composite approach was used. A quantitative image analysis (QIA) was applied to coating microstructures. Then, a 2D finite-element mesh was created from SEM images of microstructures. This simulation involved all significant features such as phase distribution and defects. In addition, assumptions on microstructure properties of coating were made. However, this analysis is not significant enough since it did not give information on the interconnected network of pores and cracks. This suggests that the three-dimensional (3D) morphology of the alumina composite could have a great influence. A 3D representation of the microstructure was therefore obtained from 3D pictures using X-ray microtomography [10]. Volume tetrahedral grids were generated to simulate the properties of alumina composite [11]. The objectives of this work were the identification and contribution of every part of the alumina coating to the final properties and the study of the potential and limitations of the computational approach.

Experimental

Thermal spraying

Three types of alumina composite coating were sprayed onto grit-blasted stainless steel plates (AISI 304 L, $25 \times 30 \times 2$ mm^3, Ra $\approx$ 4 µm) with an F4-MB Sulzer Metco torch (Table 1). The scanning step and the velocity of the torch were equal to 5×10^{-3} m/pass and 0.2 m/s, respectively. Two air-cooling jets close to the torch lowered the coating temperature, prevent thermal stresses and consequently avoid adhesion problems. A commercial powder was used, i.e. 105 SFP alumina from Sulzer Metco/Wohlen.

Table 1 Plasma spraying parameters

Sample	A	B	C
Powder		105 SFP	
Mode		APS	
Intensity (A)	530	530	600
Spraying distance (mm)		130	
Ar gas (L/min)	41	30	41
H_2 gas (L/min)	14	8	14
Powder (g/min)		20	
Injector diameter (mm)		1.8	
Injection gas (L/min)		3.4	

Two-dimensional simulation

Every Al_2O_3 composite microstructure was studied using QIA of series of SEM images (LEO1450VP). To meet criteria for statistics, 15 SEM digitalized images ($764 \times 1{,}024$ pixels^2) at a magnification of 1,500× were recorded per coating. Back-scattering electrons were used to enhance the image contrast of voids and defects. Cross-sectioned specimens were metallized (Au–Pd film $\approx$ 3 nm) prior to SEM acquisition. QIA consisted in multi-stage processing using “Matlab®” software [3]. An FEM based on the actual microstructure was developed using “Zebulon®”. It could be used to read pixels from the image file and group them based on their grey-scale levels. Every domain was corresponded to a specific constituent. In this work, two domains were obtained for porosity and for alumina. After the discriminating of the phases, a 2D finite-element mesh was generated. The element size was homogeneous and chosen to describe the cracks of the microstructure. The porosity volume fraction was lower than that obtained with QIA. Due to the limited capacity of the programme, some very thin cracks in QIA could not be modelled. A

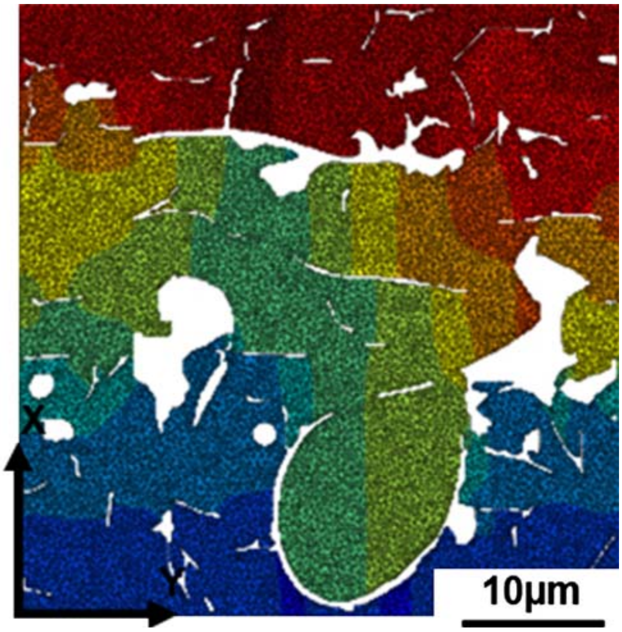

Fig. 1 Tensile test of a 2D microstructure coating mesh

compromise had to be set between the meshing and the accuracy of the microstructure. The effective in-plane Young's modulus was determined from calculated reactions caused by in-plane stretching of the model following the expression [12]: $E_{\text{eff}} = \frac{Lx \bullet \sum_x Fi}{Ly \bullet \Delta L}$, where F_i in the reaction in the node *i*th in the *x* direction; ΔL is the prescribed in-plane displacement, and L_x and L_y are the horizontal and vertical dimensions, respectively, in the model (Fig. 1). All simulations were performed in the plane strain assumption. In every simulation, the results along transverse direction were obtained by rotating the boundary conditions.

Three-dimensional simulation

The 3D structure of the alumina composite was investigated by X-ray microtomography (XMT), which was performed at the ESRF (European Synchrotron Radiation Facility) using beamline ID19. In this experiment, a collimated X-ray beam (19 keV) penetrated the alumina sample ($0.5 \times 0.5 \times 10$ mm^3) and the transmitted X-rays were recorded using a 2D detector. The Beer-Lambert law allowed the calculation of the ratio between incident and transmitted photons that result in an X-ray attenuation map through the sample. The reconstruction [13] of the 3D structure was obtained from the recording of several radiographs of the sample for different angular positions (1,500 radiographs for 180°). This technique could show all the microstructural features (pores, macrocracks, etc.). The best voxel resolution (0.28 μm) at ESRF was used to define accurately the alumina coating. After measurements and reconstruction of the volume, it was segmented to discriminate the phases in the alumina coating. Then, the 3D image was used to achieve an FEM. This consists in generating triangulated surface models with "Amira®" software [11] and build an unstructured tetrahedral mesh on the basis of this surface (Fig. 2).

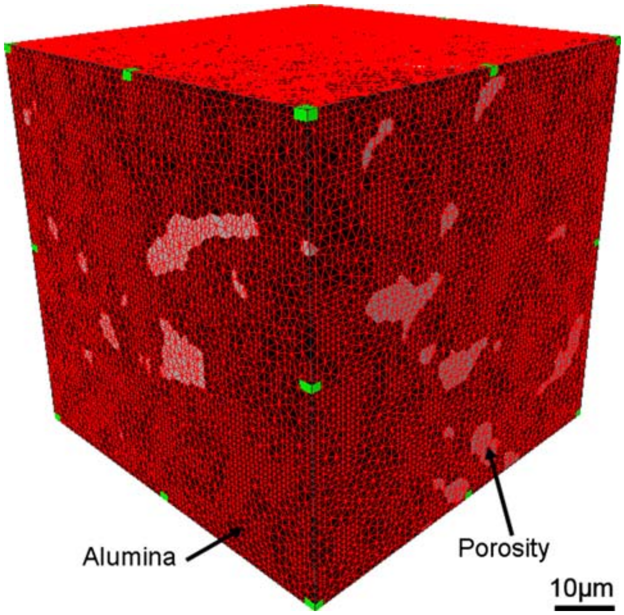

Fig. 2 3D mesh of the coating microstructure

These meshes allow the direct calculating of material properties. This model involves the concept of the representative volume element, considered as the smallest material volume, which possesses the overall properties of the composite [14]. The equivalent boundaries from 2D simulation were used in a 3D simulation to calculate the modulus. The effective Young's modulus was determined from the expression: $E_{\text{eff}} = \frac{V_{\text{Al}_2\text{O}_3}}{V} \cdot \frac{L \cdot \langle \sigma \rangle}{\Delta L}$, where $V_{\text{Al}_2\text{O}_3}$ is the volume of alumina, V the total volume (porosity and alumina), ΔL the prescribed displacement, L the horizontal or vertical dimension in the model and $\langle \sigma \rangle$ the stress average in the alumina material.

Results

Alumina material behaviour

Thermal spraying is a deposition process in which molten particles impinge at a high velocity, spread and solidify on a substrate to form thin lamellae. Consequently, thermally

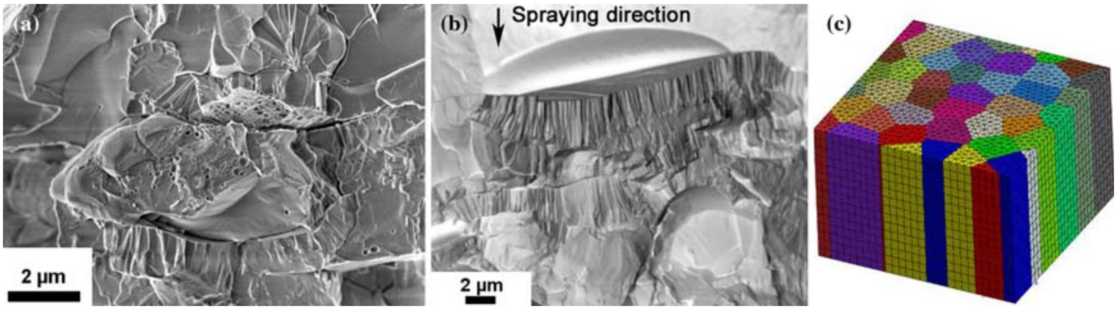

Fig. 3 Fractography of an alumina splat; (**a**) Columnar grain; (**b**) Porosity at the columnar interface; (**c**) Mesh of alumina grains

sprayed alumina coatings show a composite microstructure due to the presence of defects such as pores, inter-lamellar and intra-lamellar cracks. The alumina material behaviour was studied to develop an FE simulation of the coating microstructure. In the literature, the alumina behaviour used in FE simulation of plasma-sprayed coating is said to be isotropic (300 GPa) [8]. However, as-sprayed alumina shows a complex microstructure which cannot be considered as isotropic. X-ray diffraction did not exhibit alumina in the stable α-corumdum phase but in the metastable γ form [15]. The residual α-phase can be attributed to unmelted powder particles. This can be explained because of the rapid microscopic cooling rate, as ascertained by the γ-columnar splat microstructure (Fig. 3). An Na-rich phase was detected in some splats too. Na came from the starting powder where some particles had been polluted during the powder production process. Moreover, a crystallographic texture analysis showed a preferential orientation (30%) of the crystal plane perpendicular to the spraying direction at the top of the coating. This texture vanished near the substrate. The process parameters led to the material texture. High heating during spraying coupled with the alumina low conductibility resulted in a low macroscopic cooling. The orientations of grains, which allow the release of calories (i.e. in the spraying direction), were promoted. This texture was confirmed by measurements of the elastic modulus using nanoindentation. Several authors used this technique to characterize the mechanical properties of coatings [14, 16]. An orthotropic behaviour was established for γ-alumina between the spraying direction ($E_{\mathrm{SP}} = 194$ GPa) and transverse direction ($E_{\mathrm{TD}} = 224$ GPa). A difference in the modulus was exhibited between stable ($E_{\alpha-\mathrm{SP}} = 286$ GPa) and metastable alumina ($E_{\gamma-\mathrm{SP}} = 224$ GPa). Then, the Na-rich splats showed the lowest modulus (187 GPa). All characteristics confirmed the complex behaviour of alumina (Fig. 3c). In this paper, only the behaviour of γ-alumina was used to simulate the coating microstructure. The complete behaviour was obtained by an FE simulation of 50 grains in alumina. FE meshing of the microstructure fits the columnar morphology and texture of alumina splats. The elastic constants of the ideal dense γ-alumina single crystal (in Voigt notation, the stiffness constants were $C_{11} = 319$ GPa, $C_{12} = 153$ Gpa, $C_{44} = 163$ GPa) have been found in the literature [15]. In order to determine the stiffness matrix of γ-alumina, a kinematic unifom boundary condition was used. This matrix took into account the orthotropic behaviour of alumina:

$$C = \begin{pmatrix} 382 & 111 & 131 & & & \\ 111 & 378 & 135 & & & \\ 131 & 135 & 357 & & & \\ & & & 141 & & \\ & & & & 136 & \\ & & & & & 113 \end{pmatrix}$$

The difference between the modulus from numerical calculation ($E_{\mathrm{TD}} = 307$ and $E_{\mathrm{SP}} = 290$ GPa) and nanoindentation ($E_{\mathrm{TD}} = 224$ and $E_{\mathrm{SP}} = 190$ GPa) can be attributed to the boundary conditions and the fine grain morphology. Periodic conditions could improve the results from numerical simulations [17]. Moreover, the splat substructure (Fig. 3b) showed cracking between columns

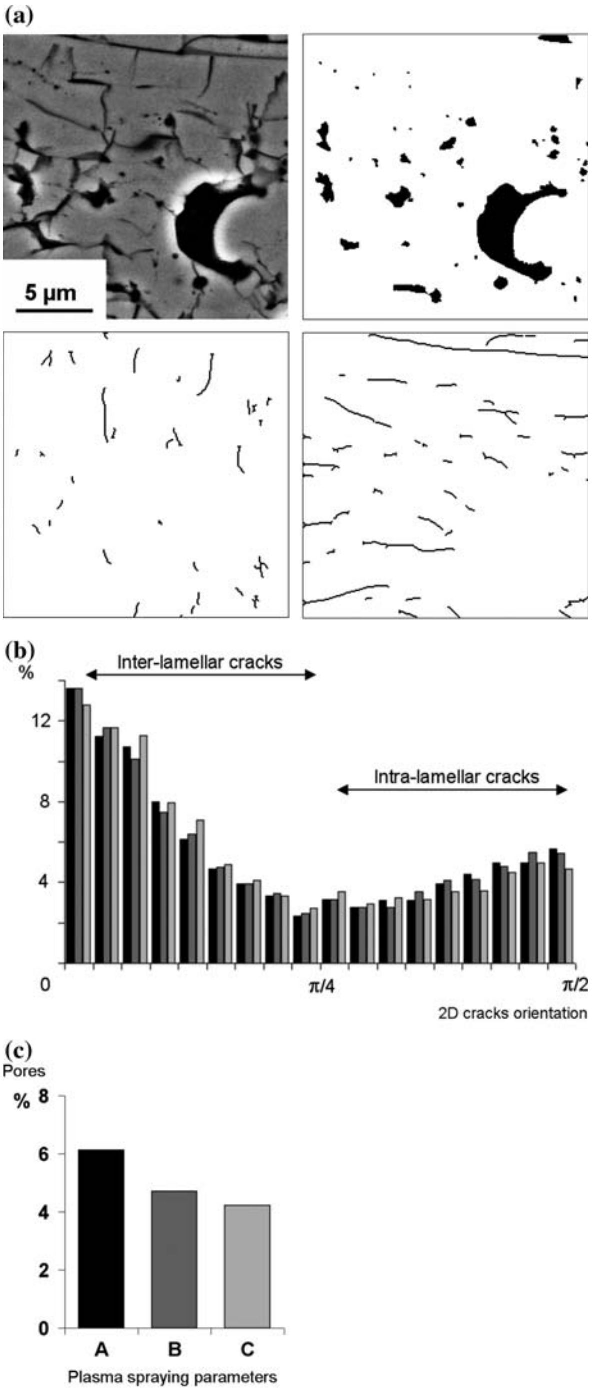

Fig. 4 Microstructure analysis (**a**) QIA processing stages (**b**) 2D crack density (**c**) 2D pore density

plus porosity coalescence at the columnar interface which decreased the elastic constant of alumina [18]. In this paper, the coating simulations were made with the numerical behaviour of γ-alumina.

Two-dimensional approach to alumina coating

The SEM mapping and QIA showed three parts in the 2D approach: the alumina nature, the pores and the cracks (Fig. 4). The difference between inter and intra-lamellar cracks was involved. The process parameters led to different levels of pores and cracks. The inter-lamellar crack density was always higher than that of intra-lamellar cracks. Microstructure variation can be attributed to the melting state of the powder in the plasma torch, which influenced the particle impinging during the spraying process. All these types of microstructures allowed develop the 2D FE simulation of microstructure. The optimal alumina representative area (a square image of 71 μm^2) was determined from QIA at different image scales. This area corresponds to three plasma torch passes to build-up the coating. An anisotropy could be exhibited since the elastic modulus in the spraying direction was lower than that in the transverse direction (Fig. 5a). Moreover, the effective Young's modulus in the two directions decreased when increasing total porosity. Mechanical simulation exhibited two parameters to study the alumina coating microstructure. Cracks length and pore distribution influenced the mechanical properties of coatings. For example, for microstructures with similar volumes and distributions of pores but with different crack lengths, a decrease in the modulus from 90 to 60 GPa was found (Fig. 5b).

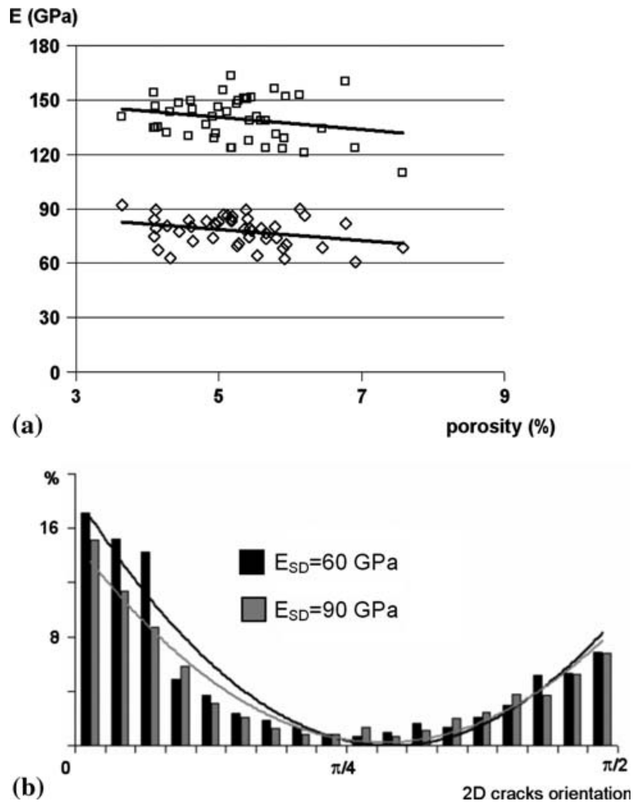

Fig. 5 (**a**) 2D Young's modulus in spraying and transverse directions (**b**) Crack density influence

Three-dimensional approach to alumina coating

The 3D microstructure from X-ray tomography showed only the pores and the alumina matrix. The resolution of the technique limited to 0.5 μm^3 the size of the defects, which could be detected (Fig. 6).

The 3D characterization was based on the work by Parra Denis et al. [19] in which a method was developed to carry out a 3D shape analysis using morphological criteria. The distribution size and the volume of pores were calculated for different process parameters. The results did not show the same trend as that from the 2D approach (Fig. 7b) when

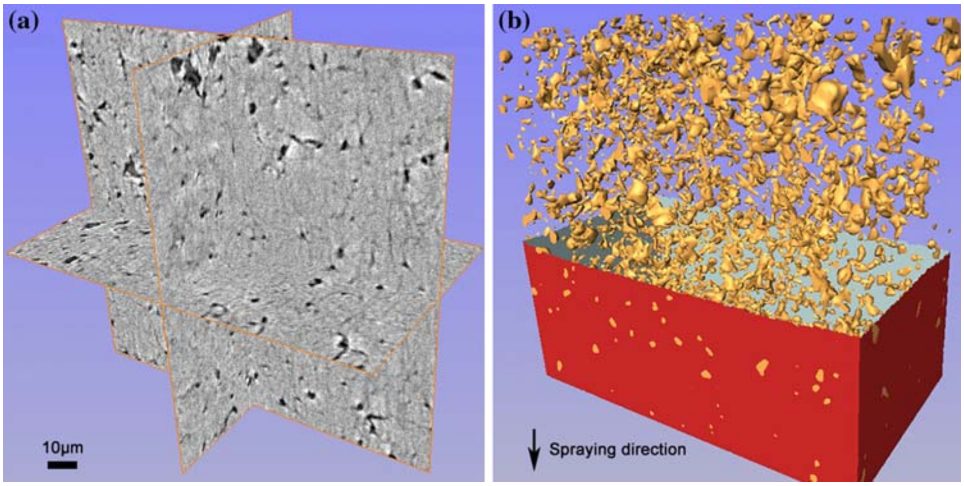

Fig. 6 Complex 3D porosity in an alumina coating (56 μm^3), (**a**) Microtomography analysis, (**b**) 3D quantitative image analysis

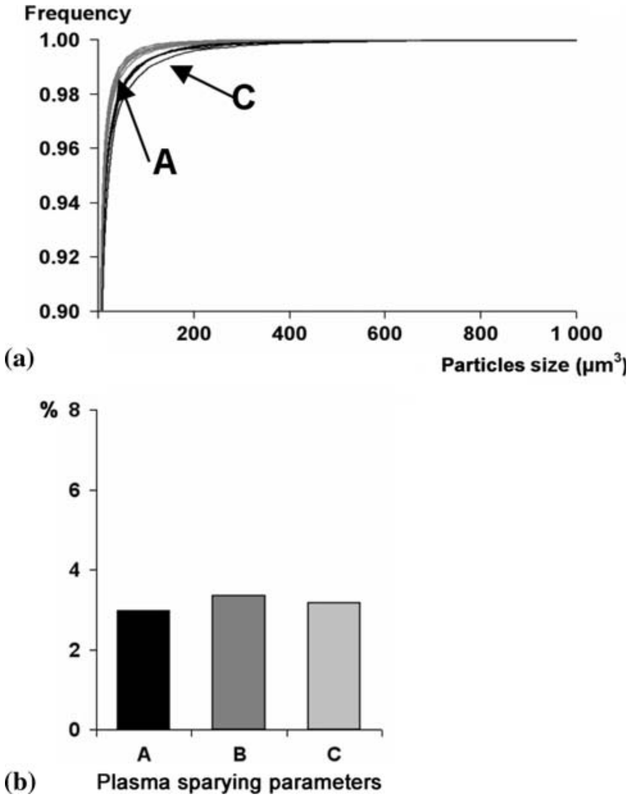

Fig. 7 (**a**) Histogram of pores (**b**) 3D porosity as a function of plasma parameters

comparing process parameters. Moreover, porosity density was shown to be lower than that from the 2D analysis. Figure 7a shows that 90% of the pores have a volume lower than 100 µm^3. Moreover, no percolation between pores was found in the 3D microstructure.

A mass distribution parameter was used to characterize the morphology of pores in coating. The moments of inertia of an object depend on its shape and characterize the distribution of mass within the shape. They correspond to the eigenvalue in the inertia matrix of the shape. The normalized moments are defined as: $\lambda_i = I_i/(I_1 + I_2 + I_3)$, $i = 1,2,3$, where I_i are the moment of inertia. Their sum is equal to 1 and they are ranked as: $\lambda_1 > \lambda_2 > \lambda_3$. From those equations and the definition of inertia moments, the two following expressions could be inferred: $\lambda_i \leq 0.5$ and $\lambda_2 \geq 0.5(1 - \lambda_1)$. These equations led to the 3D shape of pores in 2D plane graph (Fig. 8).

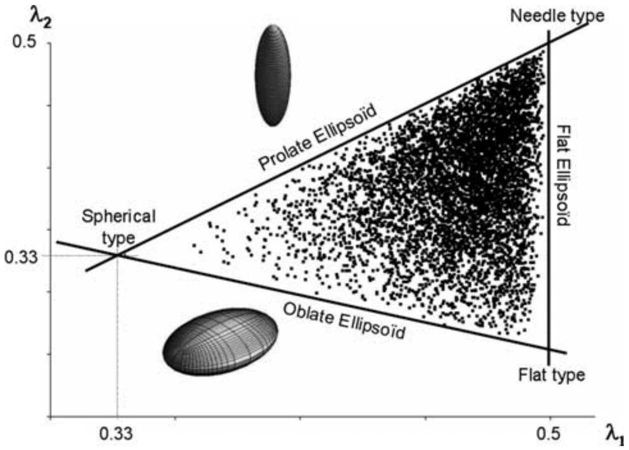

Fig. 8 3D pores morphologies

Three types of mass distribution were exhibited,: i.e, spherical, flat and needle. Along the figure borderlines, shapes are prolate ellipsoid, oblate ellipsoid or flat ellipse type. The pores did not show a spherical shape. The mass distribution was similar to needle (Fig. 8). In order to know the orientation of the pores in the alumina material, a stereographical representation was used. The 2D stereographical plot of the principal axis of inertia for the whole particle (Fig. 9) showed that particles showed an orientation parallel to the spraying axis.

Then 3D simulations of elastic properties were carried out for a volume of 45 µm^3. Young's modulus in the spraying direction was 250 GPa.

Fig. 9 Stereographical plot of the principal axis of inertia

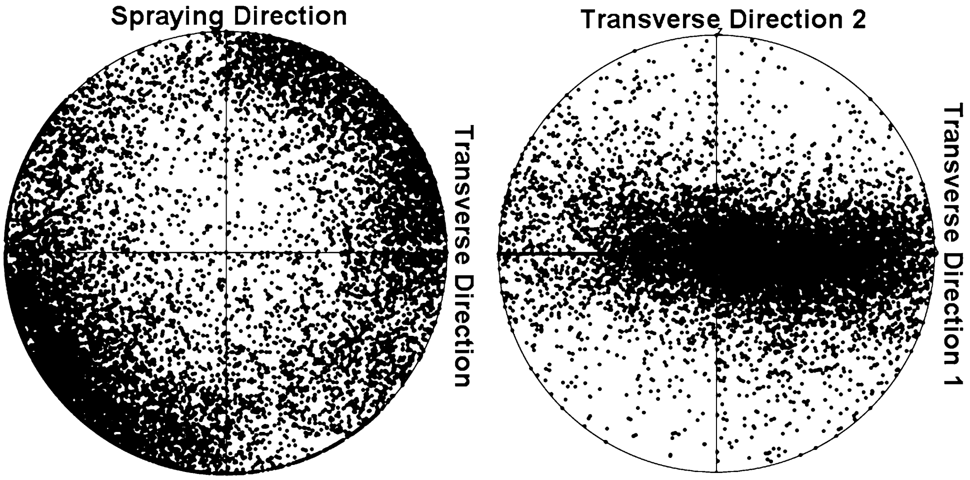

Discussion

For actual modelling of porous materials, well-defined and precise microstructural features must be involved in the model to reflect the real microstructure. The 2D approach could describe well the microstructure because it takes into account the total porosity of the alumina coating. The pores as well as the cracks were modelled (spatial resolution of about 0.0735 μm^2). In the 3D approach, only pores could be detected because of a larger resolution (0.28 μm^3). Even though the cracks were involved in the analysis, the rather large grey level area which surrounded the cracks did not permit to detect such defects (Fig. 10). This difference could explain the change in the pore density in 2D ($V_{pore} > 4\%$) and 3D ($V \approx 3\%$) analyses.

However, a 2D approach assumed a symmetry in the coating morphology, which could be applied to the cracks because of the plasma-spraying process. Build-up defects and entrapped gas generated specific inter-lamellar cracks perpendicular to the spraying direction. As for the pores, a 3D morphological analysis showed that a 2D assumption could not be applied. Pore orientations were parallel to the spraying direction, which was not involved in the 2D analysis. In a Young's modulus simulation, this simplifying assumption was valid because the cracks showed a greater influence than pores in dense coating ($V_{pore} < 4\%$). Tensile tests experiment made on samples obtained with parameters A (2D-porosity $\approx 6\%$) and C (2D-porosity $\approx 4\%$) (see Fig. 6), resulted in 100 and 130 Gpa, respectively, for spraying and transverse modulus. The 2D simulation gives a Young's modulus between 120 and 150 GPa depending on porosity. The difference between experiments and simulation can be attributed to the alumina behaviour. Grain simulation showed the orthotropic behaviour of alumina, but it was not very significant because of the presence of pores and cracks in microstructure. Better characterization of the bulk alumina behaviour could improve the simulation.

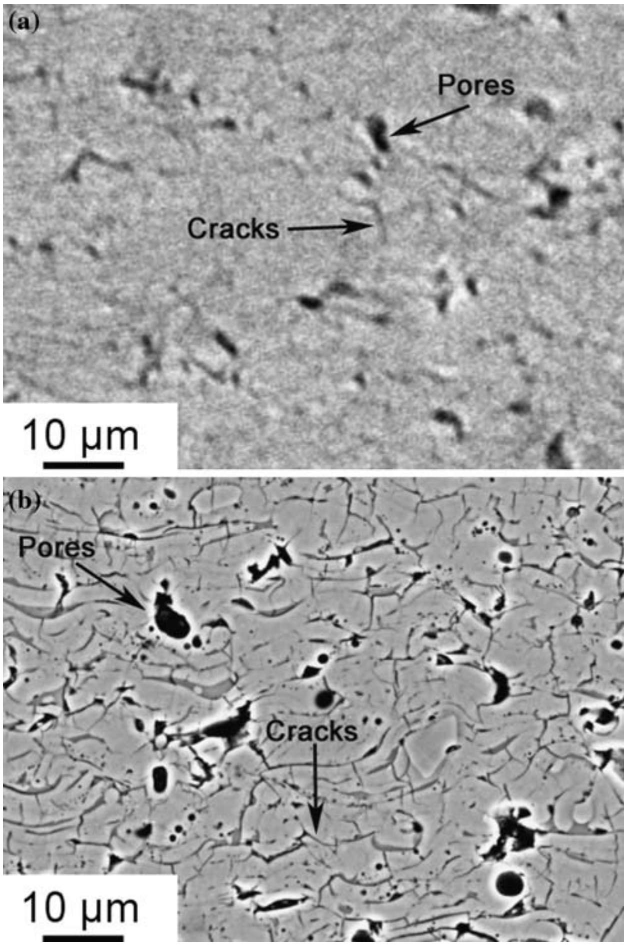

Fig. 10 (**a**) Slice from microtomography analysis (**b**) SEM cross-sectional image of plasma-sprayed alumina

Conclusion

A 2D microstructure simulation was demonstrated to be suitable for characterizing mechanical properties of alumina coating. Results obtained from 2D image analysis allowed to mesh porosity in a plasma-sprayed microstructure. This 2D simulation showed a greater influence of cracks in the spraying direction compared to that of in the transverse direction. Results obtained from 2D analysis were complemented with those obtained with XMT observation. The limits of a 2D computational approach were discussed. The 3D analyses showed the pores with an orientation parallel to the spraying direction which could not be taken into account in a 2D analysis. These analyses have a great importance to simulate the stress concentration in the coating or to determine electrical properties. This work exhibited the complementarities between 2D and 3D descriptions of the real microstructure to simulate the properties of a plasma-sprayed coating.

References

1. Gadow R, Killinger A, Voss A, Friedrich C (1998) Proceedings of the 15th international thermal spray conference, Nice, p 1083
2. Pawlowski L (1988) Surf Coat Technol 35:285
3. Beauvais S, Guipont V, Jeandin M, Juve D, Treheux D, Robisson A, Saenger R (2005) J Electroceramics 15:65
4. Li CJ, Ohmori A (2002) J Therm Spray Technol 11:365
5. Beauvais S, Guipont V, Borit F, Jeandin M, Espagnol M, Khor KA, Robisson A, Saenger R (2004) Surf Surf Coat Technol 183:201
6. Sarikaya O (2005) Surf Coat Technol 190:388
7. Bolelli G, Cannillo V, Lusvarghi L, Manfredini T, Montorsi M (2005) Surf Coat Technol 201:474
8. Wang Z, Kulkarni A, Deshpande S, Nakamuri T, Herman H (2003) Acta Mater 51:5319

9. Sevostianov I, Kachanov M (2001) Mater Sci Eng A 297:235
10. Kulkarni A, Goland A, Herman H, Allen A, Ilavsky J, Long G, De Carlo F (2005) J Therm Spray Technol 14:239
11. Madi K, Forest S, Boussuge M, Gailliegue S, Lataste E, Buffiere JY, Bernard D, Jeulin D (2007) Comput Mater Sci 39:224
12. Michlik P, Berndt CC (2006) Surf Coat Technol 201:2369
13. Feldkamp LA, Davis LC, Kress JW (1984) J Opt Soc Am 6:612
14. Ctibor P, Bohac P, Stranyanek M, Ctyrtlik R (2006) J Eur Ceramic Soc 26:3509
15. Boch P, Gault C, Platon F (1983) In: Vincenzini P (ed) Proceedings of the 5th international meeting on modern ceramics technologies, Lignano Sabbiadoro, p 825
16. Pharr GM, Olivier WC, Brotzen FR (1992) J Mater Res 7:613
17. Houdaigui ELF, Forest S, Gourgues AF, Jeulin D (2005) Proceedings of the IUTAM symposium, Beijing, p 171
18. Damani RJ, Wanner A (2000) J Mater Sci 35:4307
19. Parra Denis E, Barat C, Jeulin D, Ducottet C (2007) Mat Charact (in press)